Stabilization of ferroelastic charged domain walls in self-assembled BiFeO₃ nanoislands ⊕✓

Special Collection: Domains and Domain Walls in Ferroic Materials

Mingfeng Chen ⓘ ; Jing Wang ⓘ ; Ruixue Zhu; Yuanwei Sun; Qinghua Zhang; Ji Ma; Yue Wang; Lin Gu; Peng Gao; Jing Ma ✉ ; Ce-Wen Nan ✉ ⓘ

Check for updates

View Online   Export Citation   CrossMark

Articles You May Be Interested In

Control of binary states of ferroic orders in bi-domain BiFeO₃ nanoislands

Appl. Phys. Lett. (May 2020)

Observation of center-type quad-domain structures in ordered BiFeO₃ nanoisland arrays fabricated via mask-assisted pulsed laser deposition

Journal of Applied Physics (April 2023)

Mask assisted fabrication of nanoislands of BiFeO₃ by ion beam milling

Journal of Applied Physics (April 2013)
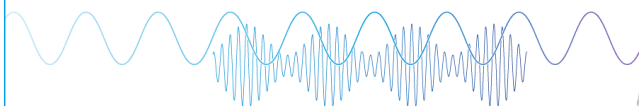
Stabilization of ferroelastic charged domain walls in self-assembled BiFeO₃ nanoislands Ⓕ

View Online   Export Citation   CrossMark

Mingfeng Chen,[1] ⓘD Jing Wang,[1,2] ⓘD Ruixue Zhu,[3,4] Yuanwei Sun,[3,4] Qinghua Zhang,[5] Ji Ma,[1,6] Yue Wang,[1] Lin Gu,[5]
Peng Gao,[3,4] Jing Ma,[1,a] and Ce-Wen Nan[1,a] ⓘD

AFFILIATIONS

[1]State Key Laboratory of New Ceramics and Fine Processing, School of Materials Science and Engineering, Tsinghua University,
Beijing 100084, People's Republic of China
[2]Advanced Research Institute of Multidisciplinary Science, Beijing Institute of Technology, Beijing 100081, People's Republic of China
[3]Electron Microscope Laboratory, School of Physics, Peking University, Beijing 100871, People's Republic of China
[4]International Center for Quantum Materials, Peking University, Beijing 100871, People's Republic of China
[5]Beijing National Laboratory for Condensed Matter Physics, Institute of Physics, Chinese Academy of Science, Beijing 100080,
People's Republic of China
[6]School of Material Science and Engineering, Kunming University of Science and Technology, Kunming, Yunnan 650093,
People's Republic of China

Note: This paper is part of the Special Topic on Domains and Domain Walls in Ferroic Materials.
[a]**Authors to whom correspondence should be addressed:** ma-jing@tsinghua.edu.cn and cwnan@tsinghua.edu.cn

ABSTRACT

Understanding the microscopic origin of exotic domain configurations and emergent properties in charged domain walls is essential for both fundamental physics and applications in next-generation nanoelectronics. In self-assembled BiFeO₃ nanoislands, 71° ferroelastic charged domain walls were spontaneously formed, which were traditionally regarded as unstable architectures. Here, by combining scanning transmission electron microscopy, geometric phase analysis, and energy dispersion spectrum, we explored the microscopic mechanism of stabilizing the tail-to-tail charged domain walls with upward center-divergent quad-domain structures in BiFeO₃ nanoislands. The comprehensive factors include the fully relaxed rhombohedral phase in nanoislands, negative surface screening charges, and upward built-in bias at the BiFeO₃-(La,Sr)MnO₃ interface, which are respectively induced by interfacial periodic dislocations, surface reconstructions, and interfacial terminations. Moreover, the unusual polarization state and domain-wall arrangement in the nanoislands were also proved to be stable even at an elevated temperature.

I. INTRODUCTION

Domain walls, accompanied with discontinuous polarization and lattice distortion, provide us with a good platform to understand coupling behavior among different order parameters[1] and the emergent physical phenomena such as multiferroicity[2] and topological chirality.[3] Since the discovery of conductive ferroelectric domain walls in multiferroic BiFeO₃ (BFO) thin films,[4] much emphasis has been placed on this field.[1,5] One of the main concerns is the intrinsic origin of high conductivity at domain-wall regions, which is generally considered the band-structure change or screening-charge accumulation.[6–8] Another research interest is to effectively

modulate the magnitude and/or polarity of domain-wall conductivity by electric field,[9–11] which has driven the development of domain-wall nanoelectronics and paved the way for future high-density data storage devices with lower power consumption. Particularly, the charged domain walls (CDWs) with head-to-head or tail-to-tail configurations have attracted much more attention and are promising to be applied in electronic devices owing to their much higher conduction (∼nA) compared to the neutral ones (∼pA).[10] In addition, since the conditions of strain, screening charges, accumulated defects, or even spin states are more complicated in CDWs,[12,13] multiple degrees of freedom can be manipulated to control the electrical
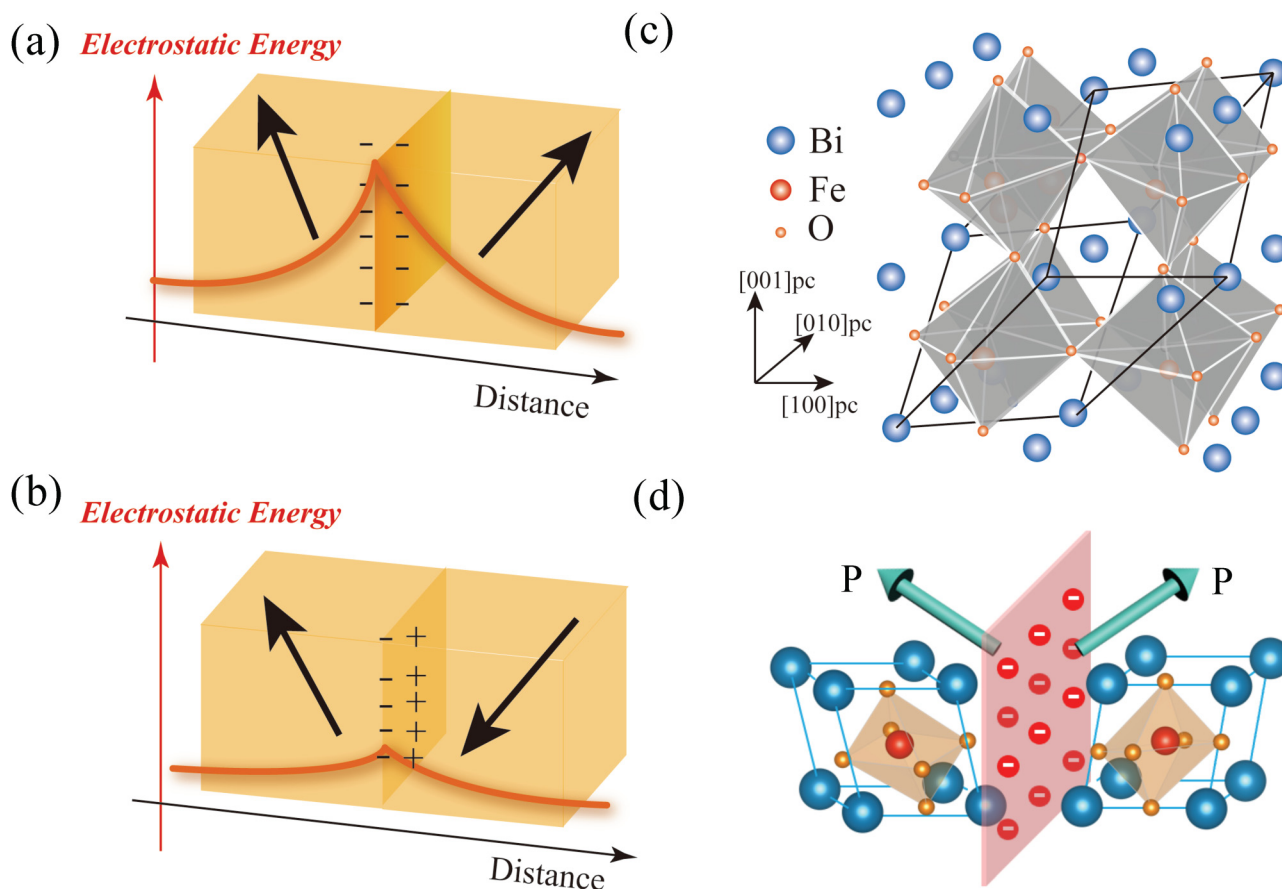
05 September 2023 02:32:44

FIG. 1. Schematic of electrostatic energy distribution around CDWs (a) and neutral domain walls (b), where the red curves represent the distribution of electrostatic energy across the CDWs and black arrows denote the polarization directions. (c) Atomic structure diagram of $BiFeO_3$. (d) Schematic of 71° CDWs in $BiFeO_3$.

conductivity and other functionalities.[14–17] However, since the electrostatic energy around the CDWs region is much higher compared with neutral domain walls [as shown in Figs. 1(a) and 1(b)], they are considered unstable and more difficult to be achieved at the pristine state.[7]

Some recent studies revealed several approaches to create and stabilize the exotic domain structures and CDWs in ferroelectrics. For example, the trailing field[18,19] resulted from the slow scanning direction of the conductive tip can be utilized to create CDWs and the injected charge from the tip can further stabilize them. In addition, CDWs and exotic domains can also be achieved in nanostructures due to shape confinement,[20] which were prepared by sacrificed nanoporous anodic alumina (AAO) template. And defects like oxygen vacancies or screening charge from environment were considered the source to stabilize those domain structures and domain walls.[16] Excitingly, our recent studies reported that 71° CDWs can be naturally formed in self-assembled BFO nanoislands on $LaAlO_3$ (LAO) substrates with $La_{0.5}Sr_{0.5}MnO_3$ (LSMO) as a buffer layer.[21,22] And specifically, this kind of CDWs also possess considerable

ferroelastic energy, which arises from the different orientation of lattice distortion in the adjacent quad-domain regions of BFO [as shown in Figs. 1(c) and 1(d)]. Therefore, it is highly desired to find out what stabilizes this conventionally believed high-energy or unstable polar texture, which can shed light on scalable functional architecture design in the future.

In this work, to figure out how 71° CDWs with upward and center-divergent quad-domains can be stabilized in BFO nanoislands, scanning transmission electron microscopy (STEM) and geometric phase analysis (GPA) were applied to analyze the microstructure and strain condition in self-assembled BFO nanoislands. Likewise, surface reconstruction and interfacial chemical terminations were also precisely studied by energy dispersion spectrum (EDS) mapping to illustrate the electrostatic condition around the nanoislands. Moreover, high-temperature piezoelectric force microscopy (PFM) further verified the robust stability of the ferroelastic CDWs as well. The thorough analysis and strategies provided in this paper might be employed to realize the highly conductive CDWs in other ferroelectrics for applications in nanoelectronics.

05 September 2023 02:32:44

II. EXPERIMENT

Sample preparation. The BFO thin films with nanoislands were prepared via pulsed laser deposition (PLD) on (001) oriented single crystal LAO substrates after 2 nm LSMO was deposited as a buffer layer. The wavelength and energy of the excimer laser for PLD were 248 nm and ~1.5 J cm^{-2}, respectively. The laser repetition rate was 5 Hz for both BFO and LSMO. LSMO and BFO films were deposited at 700 °C with the oxygen partial pressure at 0.2 mbar. After deposition was completed, the sample was cooled to room temperature at an oxygen pressure of 200 mbar with the cooling rate at 10 °C/min.

STEM and EDS. The sample for STEM was obtained by focused ion beam milling via the Precision Ion Polishing System (Model 691, Gatan Inc.). High-angle annular dark-field (HAADF) images were collected at 300 kV by using an aberration-corrected FEI Titan Themis G2 with spatial resolutions up to 60 pm. La, Al, Mn, Bi, and Fe signals were collected and mapped at the same time near the LAO/LSMO/BFO interfaces for EDS mode.

AFM characterization. Top view topography, ferroelectric domain structures of BFO nanoislands were performed in an atomic force microscope (MFP-3D, Asylum Research) using commercial conductive probes (Nanosensor). To obtain the 3D domain structures, both the vertical and lateral PFM were conducted with two in-plane sample rotation angles (in both 0° and 90°).

III. RESULTS AND DISCUSSION

As seen from the cross-sectional STEM image in Fig. 2(a), the self-assembled BFO nanoisland is trapezoid from the side view. As shown in the corresponding GPA mapping image [Fig. 2(b)], two kinds of dislocations are clearly distinguished. One category are the periodic dislocations at the LSMO/BFO interface (marked by blue arrows), and the other category are those connecting the nanoisland and uniform thin film (marked by yellow arrows). The Burgers vectors of those two kinds of dislocations are along the [100] and [110] crystalline axes, respectively.

To further investigate the dislocations at the atomic scale, the enlarged image near the BFO/LSMO interface was also obtained as shown in Fig. 2(c). The dislocations were labeled by white arrows, and their periodic space is ~8.7 nm. The periodic dislocations at the BFO/LSMO interface successfully stimulate the nucleation of rhombohedral (R)-phase nanoislands,[22] which are fully strain-relaxed as indicated by the enlarged atomic structure in the inset of Fig. 2(c) and the GPA mapping in Fig. 2(d). With benefit from the ⟨111⟩-oriented spontaneous polarizations in R-phase BFO and the
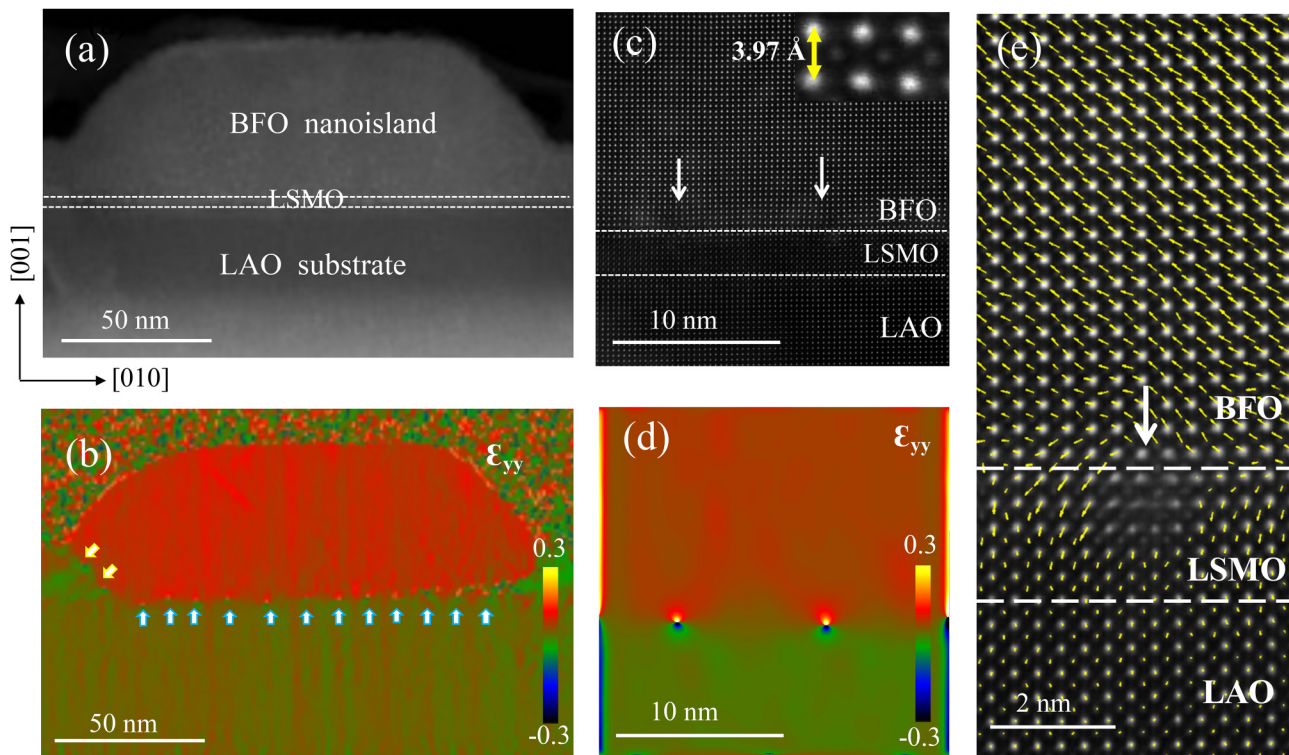

FIG. 2. Strain and dislocation characterization in self-assembled BFO nanoislands. (a) Cross-sectional STEM image of BFO nanoislands and (b) the corresponding GPA analysis, where the dislocations are marked by blue and yellow arrows. (c) Enlarged image near the BFO/LSMO interface and (d) the GPA analysis, where interface dislocations are marked by white arrows. The inset in (c) is the enlarged atomic-resolved image of R-phase nanoislands, where the bright and the darker sphere represent Bi and Fe, respectively. (e) Polarization mapping near the BFO/LSMO/LAO interface, where the direction and length of yellow arrows represent the direction and relative values of polarizations vectors in thin films.

fourfold symmetry of the square-shaped nanoislands, quad-domains with adjacent 71° ferroelastic domain walls are favored in the as-grown state. In addition, as shown in the polarization mapping near the LSMO/BFO interface in Fig. 2(e), it is clear that B-site displacement is also induced in the LSMO layer near the dislocation. The polarization in the LSMO layer is most likely attributed to the large crystal-structural deformation resulted from the strong strain field around dislocations as indicated in Fig. 2(d).[23] So, the continuous displacement transition from LSMO to BFO can effectively maintain the polarization in the BFO layer from the first unit cell at the BFO/LSMO interface and suppress the ferroelectric dead layer. Therefore, interface dislocations cannot only stabilize 71° ferroelastic domain walls by significantly decreasing the elastic strain, but also have negligible influence on the polarization distribution in BFO nanoislands.

As the BFO nanoisland has provided a suitable platform for 71° ferroelastic domains in view of strain conditions, the specific polarization direction of each quad-domain and the corresponding domain-walls type (head-to-tail, head-to-head, or tail-to-tail) are mostly dependent on the electrostatic conditions. The out-of-plane polarization vector for a ferroelastic quad-domain can be either upward or downward.[11,19] For illustration, upward center-divergent polarizations are stabilized as schematically shown in Fig. 3(a). As presented in polarization mapping near domain walls [marked by black box in Fig. 3(a)] in Fig. 3(b), the tail-to-tail 71° domain structure is clearly observed with the width of the domain wall around 3–5 nm. As for this exotic polarization state, bound charge at the surface of nanoislands is positive [Fig. 3(a)] and there should be negative screening charge to keep electric neutrality. In order to explain why this polarization configuration is stable, the HAADF images presented in Figs. 3(c) and 3(d) were collected at the nanoislands where yellow and red boxes are marked, respectively. Unlike the conventional uniform and smooth surface in epitaxial thin films,[24] surface reconstructions on both sides of nanoislands are clearly observed, which are highlighted by horizontal arrows in Figs. 3(c) and 3(d). The enlarged image of this surface reconstruction is also presented in the inset of Fig. 3(d) for a better view, and the surface Bi_2O_3 layer can be identified clearly. According to the previous study,[25] this Bi_2O_3 layer plays an essential role in stabilizing the upward polarization in two ways. On the one hand, the negative screening charge can result from the change of the ionic charge of Bi atoms at the surface. The ionic charge of Bi would decrease to a great extent in the top Bi_2O_3 monolayer (around +1.27 according to the first principle calculations by Pan and
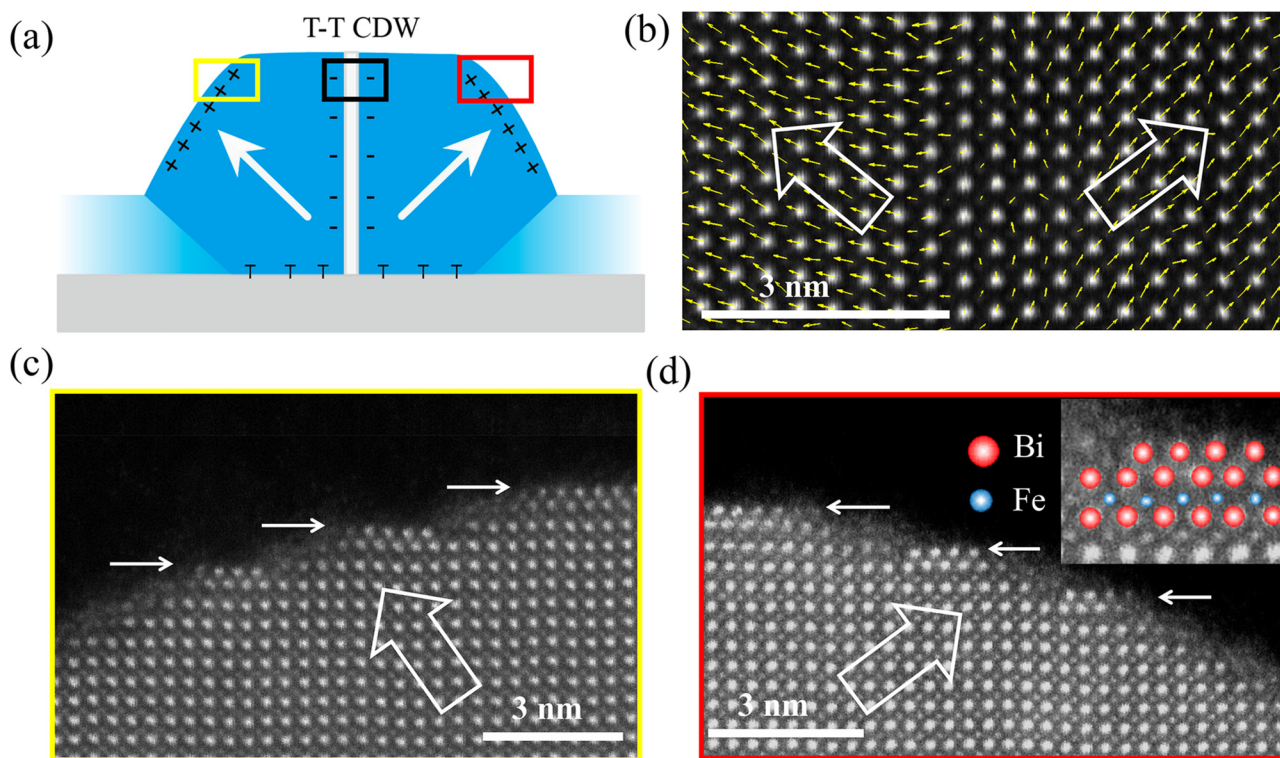
FIG. 3. Surface reconstructions of the BFO nanoislands. (a) Schematic diagram of polarization states and bound charge of nanoislands. (b) Polarization mapping near CDWs, where the length and angle of yellow arrows represent the value and direction of polarization, respectively. (c) and (d) HAADF image of the left and right corner near the surface of the nanoislands. These two parts are marked by yellow and red boxes in the schematic diagram (a), respectively. The horizontal arrows indicate BiO monolayer and the inset in (d) shows the amplified atomic structure of the surface layer.
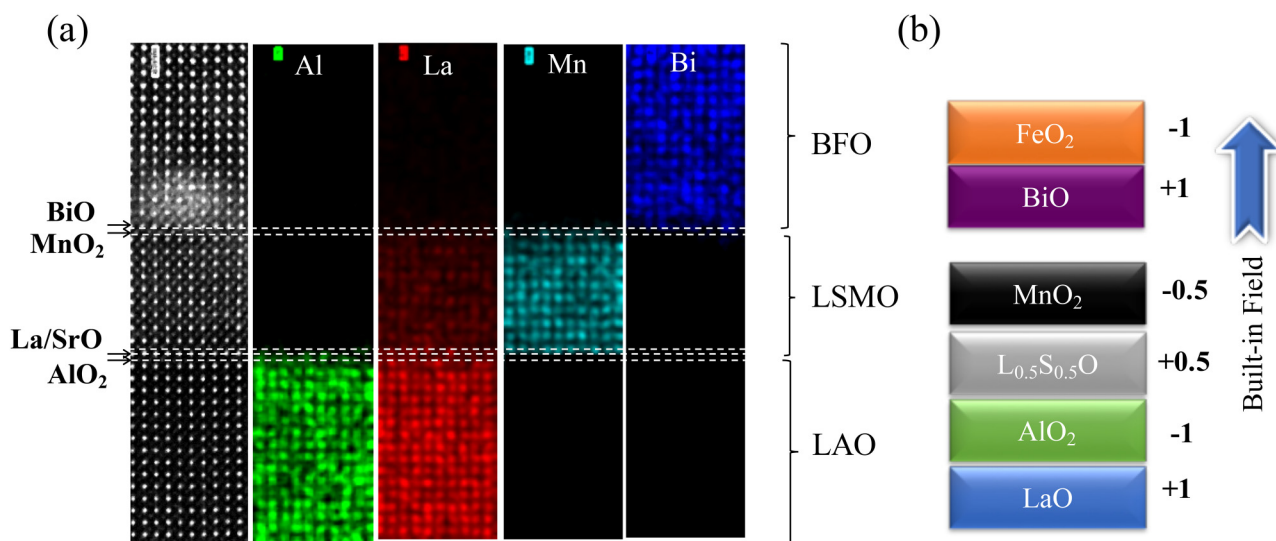
FIG. 4. Interface terminations and stacking sequence. (a) From left to right: HAADF, Al, La, Mn, and Bi EDS images near the BFO/LSMO/LAO interfaces. (b) Schematic diagram of the stacking sequence of BFO/LSMO/LAO.
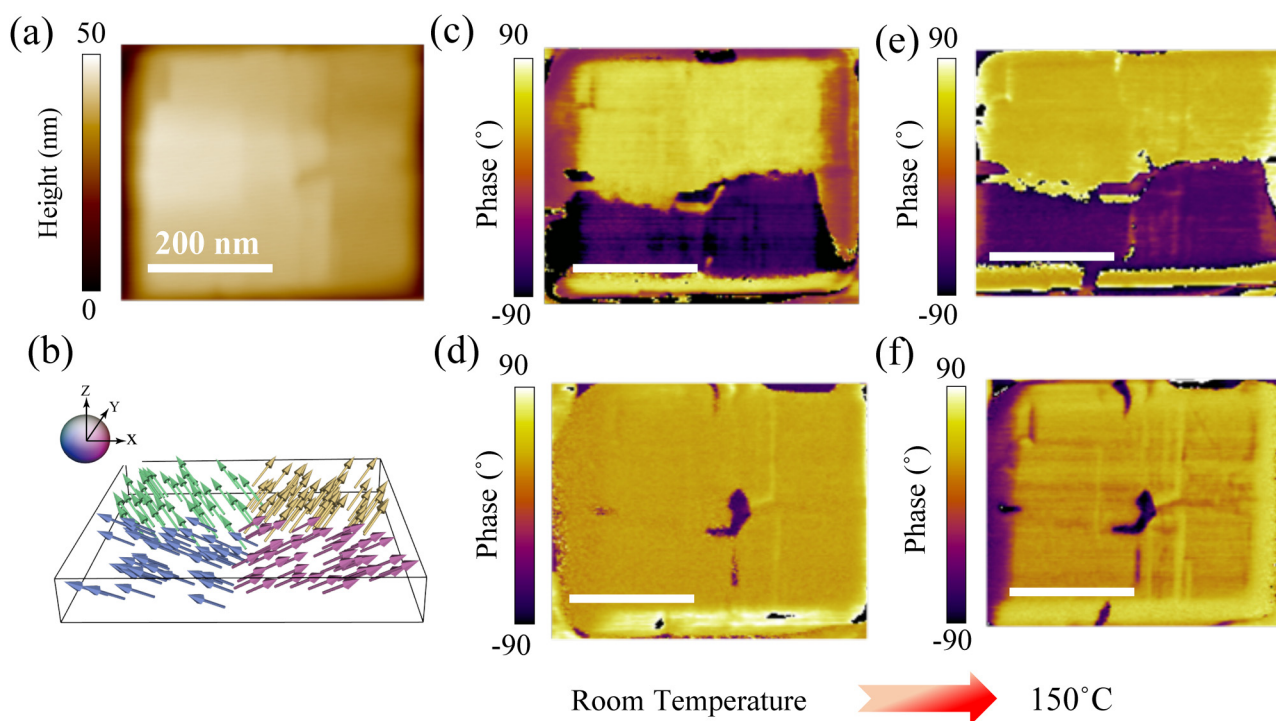
FIG. 5. Stability of domain configurations and CDWs at high temperature. (a) Topography of the BFO nanoislands. (b) Schematic of the 3D polarization state in the BFO nanoislands. In-plane [(c) and (e)] and out-of-plane [(d) and (f)] phase images of the nanoislands at room temperature and 150 °C, respectively.

co-workers[25]), which therefore could provide the negative screening charge and stabilize the upward polarizations. On the other hand, the different Bi–O bond strength in the vicinity of nanoisland surface and in the inner part would lead to a strong dipole field pointing to the surface of nanoislands and effectively counteract the depolarizing field in the opposite direction. And because the reconstructed BiO layers were symmetrically formed on both sides of the nanoislands [Figs. 3(c) and 3(d)], they could exert identical above-mentioned effects on adjacent quad-domains, thus keeping the tail-to-tail CDWs stable.

In addition to the surface part, LSMO/BFO interface terminations can also be engineered to tune the electrostatic potential and built-in field which can further modify the polarizations in BFO.[26,27] In our experiments, the LAO substrate was annealed at 1100 °C for 2 h and obtained the fully AlO_2 terminated surface with atomically flat terraces before LSMO and BFO were deposited. Figure 4(a) presents the atomically resolved HAADF and the corresponding EDS mappings near the BFO/LSMO/LAO interface. The EDS images for Al, La, and Mn can further confirm that the LAO substrate is terminated at the AlO_2 plane and the stacking sequence is AlO_2-$(La_{0.5}Sr_{0.5})O$-MnO_2 at the LSMO/LAO interface. As a result, when BFO was further deposited on the LSMO layer, the stacking sequence is $(La_{0.5}Sr_{0.5})O$-MnO_2-BiO-FeO_2. According to previous studies, interface polar discontinuity induced charge transfer and polar field could effectively control the polarization states. Within the frame of the polar discontinuity model,[28,29] the charge density at the MnO_2-terminaed interface is $+0.5e/-0.5e/+1e/-1e$ [Fig. 4(b)], resulting in the positive charge of $0.25e$ $(0.5e/2-0.5e+1e/2)$ at the interface and finally leads to the dipole pointing from the LSMO to BFO layer attributed to Thomas Fermi screening.[30] More importantly, even this interface dipole is strongly correlated with interface stacking sequence, this effect is robust with thickness in the range of 10–150 nm, which is consistent with the phenomenon in the BFO nanoisland with the height around 40 nm. Therefore, the upward built-in field induced from interface terminations could further maintain the upward center-divergent polarization state.

The analyses above have explained that the 71° ferroelastic charged domain walls can be obtained in self-assembled BFO nanoislands in terms of elastic and electrostatic conditions. To further test the stability of this exotic domain structure for future applications in devices, temperature-dependent PFM was also carried out. Figure 5(a) is the topography of one nanoisland, and Fig. 5(b) is the schematic diagram showing the 3D polarization configuration as reported in our previous study.[21] The in-plane phase (IPP) and out-of-plane phase (OPP) images for the pristine nanoisland at room temperature are shown in Figs 5(c) and 5(d). It is clearly seen from Figs. 5(e) and 5(f) that both the IPP and OPP images remain almost unchanged when temperature goes up to 150 °C, indicating the superior stability of the pristine polarization state.

Besides the stability of CDWs at higher temperature, the stability under electric field is equally important for practical applications. Based on the previous studies, the position and conductivity of CDWs in BFO nanoislands can be rarely affected after hundreds of ferroelectric switching.[10] The CDWs can be well-retained even when each quarter of domain is switched by 180°.[21]

IV. CONCLUSIONS

In summary, the stabilization of the exotic 71° ferroelastic CDWs in self-assembled BFO nanoislands have been systematically investigated and explained in view of elastic and electrostatic conditions. By combining STEM and GPA, it was revealed that the nanoislands were fully strain-relaxed to rhombohedral phase by the periodic dislocations at the LSMO/BFO interface. Therefore, quad-domains with adjacent 71° ferroelastic charged domain walls are favored in the square-shaped R-phase nanoislands with spontaneously ⟨111⟩-oriented polarizations and fourfold symmetry. In addition, by investigating the surface reconstruction and BFO/LSMO interface terminations through EDS, the stabilization of tail-to-tail CDWs with upward and center-divergent quad-domain structures can be illustrated regarding the electrostatic condition: the BiO monolayer reconstructed on the surface can provide negative screening charge and counteract the depolarization field, while the $(La_{0.5}Sr_{0.5})O$-MnO_2-BiO-FeO_2 stacking sequence can provide an additional upward built-in field. Moreover, high-temperature PFM images also confirm the excellent stability of the ferroelastic CDWs. These findings provide practical strategies to form and stabilize the exotic domain structures and CDWs for the applications in future nano-electronics with high density and low power consumption.

AUTHORS' CONTRIBUTIONS

M.C. and J.W. contributed equally to this work.

ACKNOWLEDGMENTS

DATA AVAILABILITY

The data that support the findings of this study are available from the corresponding author upon reasonable request.

REFERENCES

[1]R. K. Vasudevan, W. Wu, J. R. Guest, A. P. Baddorf, A. N. Morozovska, E. A. Eliseev, N. Balke, V. Nagarajan, P. Maksymovych, and S. V. Kalinin, Adv. Funct. Mater. **23**, 2592 (2013).

[2]T. Lottermoser and M. Fiebig, Phys. Rev. B **70**, 220407(R) (2004).

[3]S.-W. Cheong, Natl. Sci. Rev. **6**, 624 (2019).

[4]J. Seidel, L. W. Martin, Q. He, Q. Zhan, Y. H. Chu, A. Rother, M. E. Hawkridge, P. Maksymovych, P. Yu, M. Gajek, N. Balke, S. V. Kalinin, S. Gemming, F. Wang, G. Catalan, J. F. Scott, N. A. Spaldin, J. Orenstein, and R. Ramesh, Nat. Mater. **8**, 229 (2009).

[5]G. Catalan, J. Seidel, R. Ramesh, and J. F. Scott, Rev. Mod. Phys. **84**, 119 (2012).

[6]J. Seidel, P. Maksymovych, Y. Batra, A. Katan, S. Y. Yang, Q. He, A. P. Baddorf, S. V. Kalinin, C. H. Yang, J. C. Yang, Y. H. Chu, E. K. Salje, H. Wormeester, M. Salmeron, and R. Ramesh, Phys. Rev. Lett. **105**, 197603 (2010).

05 September 2023 02:32:44

[7]E. A. Eliseev, A. N. Morozovska, C. T. Nelson, and S. V. Kalinin, Phys. Rev. B **99**, 805416 (2019).

[8]S. Farokhipoor and B. Noheda, Phys. Rev. Lett. **107**, 127601 (2011).

[9]J. Jiang, Z. L. Bai, Z. H. Chen, L. He, D. W. Zhang, Q. H. Zhang, J. A. Shi, M. H. Park, J. F. Scott, C. S. Hwang, and A. Q. Jiang, Nat. Mater. **17**, 49–56 (2018).

[10]J. Ma, J. Ma, Q. Zhang, R. Peng, J. Wang, C. Liu, M. Wang, N. Li, M. Chen, X. Cheng, P. Gao, L. Gu, L.-Q. Chen, P. Yu, J. Zhang, and C.-W. Nan, Nat. Nanotechnol. **13**, 947 (2018).

[11]Y. Zhang, J. Li, and D. Fang, J. Appl. Phys. **107**, 034107 (2010).

[12]J. H. Lee, I. Fina, X. Marti, Y. H. Kim, D. Hesse, and M. Alexe, Adv. Mater. **26**, 7078 (2014).

[13]E. A. Eliseev, A. N. Morozovska, Y. Gu, A. Y. Borisevich, L.-Q. Chen, V. Gopalan, and S. V. Kalinin, Phys. Rev. B **86**, 085416 (2012).

[14]L. Li, J. Britson, J. R. Jokisaari, Y. Zhang, C. Adamo, A. Melville, D. G. Schlom, L.-Q. Chen, and X. Pan, Adv. Mater. **28**, 6574 (2016).

[15]R. K. V. Jan Seidel and N. Valanoor, Adv. Electron. Mater. **2**(1), 1500292 (2016).

[16]G. Tian, W. Yang, X. Song, D. Zheng, L. Zhang, C. Chen, P. Li, H. Fan, J. Yao, D. Chen, Z. Fan, Z. Hou, Z. Zhang, S. Wu, M. Zeng, X. Gao, and J. M. Liu, Adv. Funct. Mater. **29**, 1807276 (2019).

[17]N. Domingo, S. Farokhipoor, J. Santiso, B. Noheda, and G. Catalan, J. Phys. Condens. Matter **29**, 334003 (2017).

[18]A. Crassous, T. Sluka, A. K. Tagantsev, and N. Setter, Nat. Nanotechnol. **10**, 614 (2015).

[19]R. K. Vasudevan, Y. Matsumoto, X. Cheng, A. Imai, S. Maruyama, H. L. Xin, M. B. Okatan, S. Jesse, S. V. Kalinin, and V. Nagarajan, Nat. Commun. **5**, 4971 (2014).

[20]Z. Li, Y. Wang, G. Tian, P. Li, L. Zhao, F. Zhang, J. Yao, H. Fan, X. Song, D. Chen, Z. Fan, M. Qin, M. Zeng, Z. Zhang, X. Lu, S. Hu, C. Lei, Q. Zhu, J. Li, X. Gao, and J. M. Liu, Sci. Adv. **3**, e1700919 (2017).

[21]M. Chen, J. Ma, R.-C. Peng, Q. Zhang, J. Wang, Y. Liang, J. Wu, L.-Q. Chen, J. Ma, and C.-W. Nan, Acta Mater. **175**, 324 (2019).

[22]J. Ma, J. Wang, H. Zhou, Q. Zhang, Y. Liang, M. Chen, L. Gu, B. Xu, J. Zhang, J. Ma, and C. W. Nan, Nanoscale **11**, 20514–20521 (2019).

[23]Z. Wang, H. Guo, S. Shao, M. Saghayezhian, J. Li, R. Fittipaldi, A. Vecchione, P. Siwakoti, Y. Zhu, J. Zhang, and E. W. Plummer, Proc. Natl. Acad. Sci. U.S.A. **115**, 9485 (2018).

[24]R. J. Zeches, M. D. Rossell, J. X. Zhang, A. J. Hatt, Q. He, C. H. Yang, A. Kumar, C. H. Wang, A. Melville, C. Adamo, G. Sheng, Y. H. Chu, J. F. Ihlefeld, R. Erni, C. Ederer, V. Gopalan, L. Q. Chen, D. G. Schlom, N. A. Spaldin, L. W. Martin, and R. Ramesh, Science **326**, 977 (2009).

[25]L. Xie, L. Li, C. A. Heikes, Y. Zhang, Z. Hong, P. Gao, C. T. Nelson, F. Xue, E. Kioupakis, L. Chen, D. G. Schlom, P. Wang, and X. Pan, Adv. Mater. **29**, 1701475 (2017).

[26]P. Yu, W. Luo, D. Yi, J. X. Zhang, M. D. Rossell, C. H. Yang, L. You, G. Singh-Bhalla, S. Y. Yang, Q. He, Q. M. Ramasse, R. Erni, L. W. Martin, Y. H. Chu, S. T. Pantelides, S. J. Pennycook, and R. Ramesh, Proc. Natl. Acad. Sci. U.S.A. **109**, 9710 (2012).

[27]D. Yi, P. Yu, Y. C. Chen, H. H. Lee, Q. He, Y. H. Chu, and R. Ramesh, Adv. Mater. **31**, 1806335 (2019).

[28]Y. Hotta, T. Susaki, and H. Y. Hwang, Phys. Rev. Lett. **99**, 236805 (2007).

[29]A. Ohtomo and H. Y. Hwang, Nature **427**, 423 (2004).

[30]Y. Hikita, M. Nishikawa, T. Yajima, and H. Y. Hwang, Phys. Rev. B **79**, 073101 (2009).

05 September 2023 02:32:44